Novel transmitter designs for magnetic resonance imaging

Aussenhofer, S.A.

1

Introduction and Outline

1

In this thesis new transmit systems for magnetic resonance imaging (MRI) have been studied in terms of novel resonator designs. Instead of trying to adapt established technologies from lower field strengths that are mainly based on lumped element designs it was the goal of this work to investigate alternative solutions. The higher field strength of the 7.0 Tesla MRI system and thus higher B_1 transmit frequency (~ 300 MHz) allows for designs and concepts to work that would have not been possible at lower frequencies. Especially dielectric resonators and their potential use in human MRI were investigated. The thesis closes with a truly novel resonator design based on plasma technology.

1.1. OUTLINE OF CHAPTERS

In chapter one a brief history of magnetic resonance imaging (MRI) is given followed by a review of classical RF coil design. The chapter continues with the introduction of the concept of dielectric resonators, their mode of operation and general design examples. The chapter closes with an introduction to plasma physics.

In chapter two a hybrid-electromagnetic-mode (HEM) resonator was designed and built for human wrist imaging at 7.0 Tesla. The idea was to build a first usable resonator using the dielectric properties and geometry of a common dielectric material (water) instead of using lumped element to design a MRI coil. This design was compared to a similar sized conventional MRI coil and is an elegant alternative design for quadrature fed transmit coils in MRI. Beside showing the proof of principle also a new mean of detuning this dielectric resonator has been found and worked out.

In chapter three a HEM resonator for 7.0 Tesla human digit imaging was investigated based on ceramics as a low loss dielectric material. Ceramics allows for more compact designs of dielectric resonators in human MRI. In this chapter it is furthermore shown that ceramic resonators can be double tuned simply by changing the boundary conditions.

In chapter four the concept of dielectric resonators based on low loss ceramics was further investigated. The dielectric resonator was now used in a different mode (transverse electromagnetic (TE) mode) that gives similar electric and magnetic fields like a loop coil. An eight channel transmit/receive array for cardiac imaging at 7.0 Tesla field strength was built from eight ceramic resonators. This design was compared to a conventional loop coil design of similar size in several human volunteers. Basic measures of the performance of the resonator were investigated and compared to the established loop coil design.

In chapter five a novel resonator design is described that uses a plasma as a resonator instead of dielectrics or lumped elements. This novel design allows for new concepts in MRI coil building. The basic principle of the working mechanisms is given as well as the proof of concept.

The thesis closes with chapter six with a general discussion. Furthermore, possible future developments based on the findings of this thesis are theorized.

1

1.2. THE HISTORY OF MAGNETIC RESONANCE IMAGING

SINCE the first experiments on the nuclear magnetic resonance (NMR) phenomena by Bloch [2] and Purcell [27] in 1946 and the first magnetic resonance imaging (MRI) experiments by Lauterbur [20] and Mansfield [21] MRI has been constantly in development. This development has helped to establish MRI as the gold standard for clinical imaging and provide ever better insight into the human body for diagnosis, understanding and hopefully to cure diseases.

The number of MRI examinations carried out per year in the Netherlands has been steadily increasing and is now in the order of 50 exams per 1000 population [23]. The increased need for examinations in the number of exams is not only due to an ageing population but also to the ever increasing efficiency of modern MRI machines that allow for new diagnostics and stratification.

Efficiency in MRI is proportional to the signal-to-noise ratio (SNR) [32]. The higher the SNR that a system can deliver, the faster a patient examination can be completed. Consequently, since the 1970's when Philips set out to produce a first MRI system, it has been a goal of the scientific community to increase the signal-to-noise-ratio (SNR). One way of improving the SNR is to increase the main magnetic field strength (B_0). Currently the standard clinical B_0 magnetic field strengths are 1.5 and 3.0 Tesla. In the early years of the 21st century the first 7.0 Tesla human scanners became available. It might be expected that these machines would, due to their higher magnetic field strength, inherently provide a higher SNR than their current clinical counterparts. Nevertheless, further technical development is needed for these machines to be able to deliver their full potential.

Until the introduction of 3.0 Tesla human scanners the increase of the B_0 field strength did not cause too many problems from a development perspective because the wavelength of the radio frequency (~64 MHz at 1.5 Tesla and ~128 MHz at 3.0 Tesla) of the systems used to excite the spin system was significantly longer than the dimensions of the human body. With 3.0 Tesla systems however, it was observed that although the SNR increased as would be expected due to the higher B_0, the image uniformity in some cases was not as predicted and as known from lower field MRI [9]. It soon became apparent that those image disturbances did not occur due to broken hardware of the imaging system but instead were caused by fundamental physics [37].

The number of artefacts was found to increase with increasing B_0. At 3.0 Tesla, the

presence of artefacts was to an extent that they could still be used for clinical imaging [31]. For the first 7.0 Tesla systems, the further increase in artefacts prevented their meaningful use [6, 43]. Homogeneous spin excitation within the field of view with a body coil became impossible. At higher B_0 field strengths, the corresponding electric field has a wavelength that is a fraction or a multiple of the anatomical feature being imaged. This leads to non-uniformity in the B_1 transmit field that causes shading artefacts in the images better known as dielectric effects as they can be seen in figure 1.1. To circumvent those problems it was soon understood that new means of transmit systems – preferably much closer to the anatomy – would be needed in ≥ 7.0 Tesla systems.

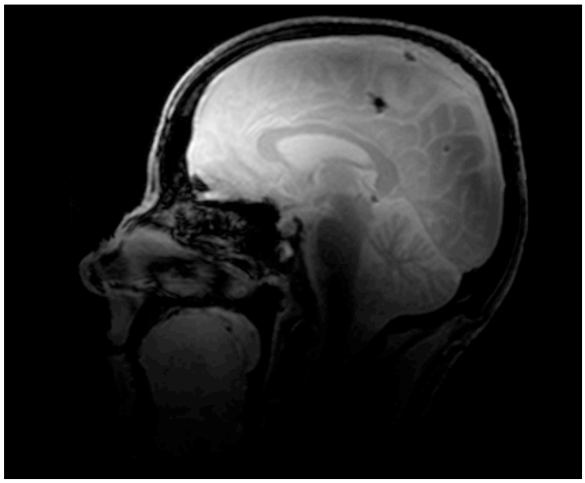

Figure 1.1: Human head MRI image acquired at 7.0 Tesla field strength. Shading artefacts can easily be seen.

A built in transmit coil (also known as a body coil on lower field systems) cannot be used with these “new” systems because interaction between high frequency transmit pulses and the human body prevents generation of a homogeneous B_1 excitation field. Instead, a local transmit and receive coil for the body part under investigation is typically used; only for imaging of body parts that are small compared to to the wavelength of the electric field, is it sometimes possible to implement, alternatively, a “simple” hardware solution, e.g. for digital imaging. Unfortunately this is seldom the case. In particular with neurological and cardiological imaging, dielectric effects cannot be adequately compensated for and new solutions are needed.

It was thus the aim of this thesis to develop novel transmitter designs for magnetic field imaging that could be used at 7.0 Tesla field strength.

1

1.3. THEORY OF MAGNETIC RESONANCE IMAGING

1.3.1. NUCLEAR SPIN AND MAGNETIC MOMENT

A magnetic resonance imaging (MRI) experiment is performed by placing an object inside a superconducting magnet, which produces a static magnetic field B_0. In this case all nuclei with a non-zero nuclear magnetic moment or nuclear spin $\vec{I}$ can be detected using MRI (the ^1H nucleus is of particular interest for reasons which are explained below). It has been shown that there is a linear relationship between the nuclear magnetic moment $\vec{\mu}$ and angular momentum $\vec{P}$

$$\vec{\mu} = \gamma \vec{P}. \tag{1.1}$$

Here γ is the proportionality constant (also known as the gyromagnetic ratio) of a nucleus.

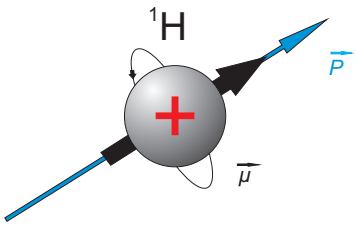

Figure 1.2: Magnetic moment of a hydrogen core.

In the classical model, rotation of a charged particle, described by its angular momentum $\vec{P}$, induces a magnetic dipole field. The direction and magnitude of this field are described by the magnetic moment $\vec{\mu}$, see figure 1.2. The vector $\vec{\mu}$ is collinear with the angular momentum $\vec{P}$ of the sphere. If a cylindrical permanent magnet is brought into an external magnetic field in order to minimize its potential energy, it experiences a mechanical torque bringing the magnet into alignment with the external field. If the magnet is rotating around its longitudinal axis it will possess angular momentum. Due to the conservation momentum the magnet cannot align parallel to the external field. Consequently, the magnet experiences a torque perpendicular both to the external field and the angular momentum, which results in rotation (precession) of the magnet. The frequency of this precession is called the Lamor frequency and corresponds to its resonance frequency $\omega_0 = \gamma B_0$.

When an external field is applied to e.g. a hydrogen-^1H nucleus, its spectral lines are split. This is also known as the Zeeman Effect. This splitting is attributed to ^1Hinteraction between the magnetic field and the magnetic dipole moment associated with the orbital angular momentum. When considering an isolated magnetic moment within a static magnetic field, one will find that transitions between the different energy levels are prohibited due to the law of energy conservation. Transitions can exclusively be induced by an additional time-dependent electromagnetic radio frequency (RF) field that interacts with the magnetic moment, the effect is known as magnetic resonance (MR).

In MRI, transitions are induced by an electromagnetic radio-frequency (RF) field $B_1(t)$ with the angular frequency ω_{RF}, which is irradiated perpendicular to the direction of the static magnetic field B_0 . Such a time-dependent magnetic field, however, can only induce transitions fulfilling the selection rule $\Delta m = \pm 1$, i.e., transitions between neighboring energy levels. As a consequence, the energy $E_{RF} = \hbar\omega_{RF}$ of a photon of the RF field must be identical with the energy difference $\Delta E = \hbar\omega_0 = \gamma\hbar B_0$ between two neighboured energy levels, which yields the resonance condition

$$\omega_{RF} = \omega_0 = \gamma B_0.$$

Due to thermal motion the magnetic moments of nuclei in a macroscopic object cancel out each other, no net magnetization is detectable. However, if this object is taken into an external magnetic field B_0 only $2I+1$ (spin levels) discrete orientations of the magnetic moments are allowed. If the object is in thermal equilibrium the spin levels are described by Boltzmann statistics:

- the lower the energy $E_m = -\gamma\hbar B_0 m$ of a state, the greater the occupation number.

The macroscopic magnetization is described by the magnetization vector M_0 which is defined as the vector sum of the nuclear magnetic moments per unit volume V. It can be calculated as

$$M_0 = |M_0| = \frac{1}{V}\sum_{i=1}^{N}(\mu_z)_i = \frac{N}{V}\cdot\frac{I(I+1)\gamma^2\hbar^2 B_0}{3k_b T},$$

where k_b is the Boltzmann's constant and $\hbar$ is the Planck's constant. This equation also explains why the enhancement of magnetic resonance imaging (MRI) is only possible by altering B_0 as T is given by the human body and γ is determined from the nucleus under investigation.

nuclei	net Spin	γ (MHz/T)
^{1}H	1/2	42.58
^{2}H	1	6.54
^{31}P	1/2	17.25
^{23}Na	3/2	11.27
^{14}N	1	3.08
^{13}C	1/2	10.71
^{19}F	1/2	40.08

Table 1.1: Nuclei, net spin and the gyromagnetic ratio for relevant nuclei in magentic resonance imaging.

The most interesting magnetic isotope for MR-imaging is the ^{1}H isotope: hydrogen is present in abundance in biologic tissue (and the water therein); the ^{1}H nucleus has a large gyromagnetic ratio; and, ^{1}H has 99.98 percent natural isotopic abundance. A table of MR-relevant properties of nuclei is given in the table 1.1.

Nuclei other than ^{1}H are often referred to as X-core nuclei. As the gyromagnetic ratio is different for those nuclei than from ^{1}H they require suitable transmit and receive hardware with a working frequency different from the one of ^{1}H. These other nuclei are often interesting for spectroscopy and functional studies as kidney function or muscle properties. These x-core nuclei profit highly from higher B_0 field strength and will be more important in the future due to improvements in hardware design.

1.3.2. NUCLEUS IN A MAGNETIC FIELD

The phenomenon of nuclear magnetic resonance (NMR), on which MRI is based, was independently discovered by Bloch [2] and Purcell [27]. In the absence of an external magnetic field, the orientation of a proton's spins is random as shown in figure 1.3:

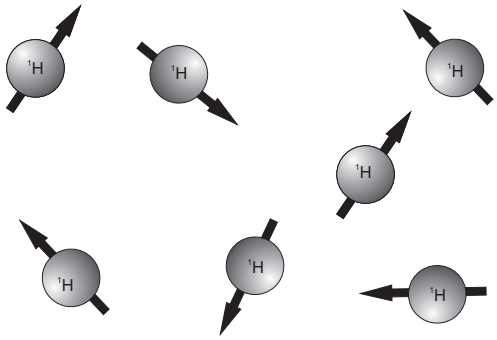

Figure 1.3: Proton spins in the absence of an outer magnetic field.

In the presence of an external magnetic field like in figure 1.4, a spinning, charged particle will behave like a small magnet and will align either parallel or anti-parallel to the direction of the B_0-field. The energies of these two spin states are similar and consequently they are similarly populated (according to a Boltzmann distribution). The parallel state has slightly lower energy: from one million protons, approx. one more is aligned parallel than anti-parallel at 1.5 Tesla.

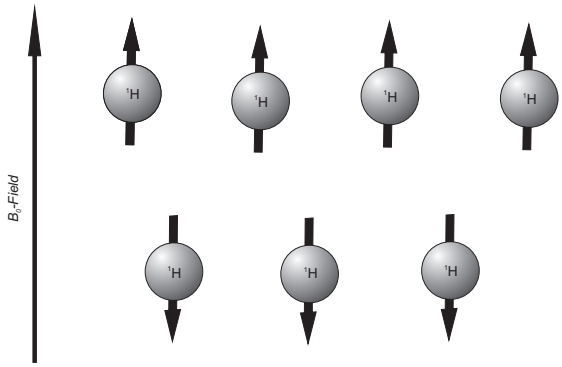

Figure 1.4: Proton spins in the presence of an outer magnetic field. There is an alignment of the spin either parallel or anti parallel to the B_0 field.

1

When aligned to an external static magnetic field, a proton will begin to precess around the direction of the static magnetic field with a frequency that is proportional to the strength of the static magnetic field, see figure 1.5. This precession can be seen as being analogous to precession of a "heavy" spinning top in the presence of gravity.

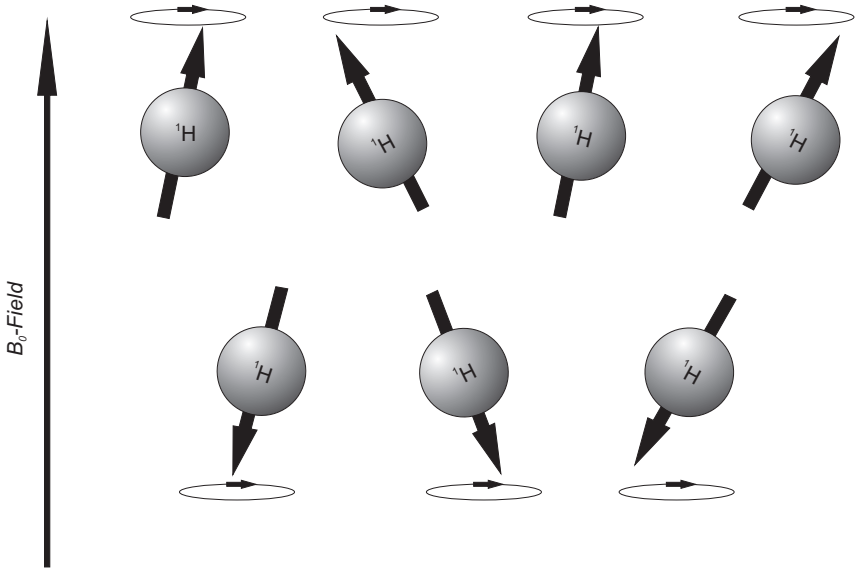

Figure 1.5: Proton spins in the presence of an outer magnetic field precessing out of phase.

In figure 1.6 a volume V containing protons is brought into an external magnetic field B_0. The proton spins form a spin system with a net magnetization represented by the vector M_0. While the nuclear magnetic moment μ can take only discrete values and angles to the B_0 vector, the magnetization vector M_0 can take any value from 0 – 180 degrees with 0 degrees representing collinear alignment and 180 degrees the anti-parallel state. A radio frequency (RF) field is then applied perpendicular to B_0 causing the protons to precess coherently, thus making it possible to detect the sum of all protons precessing as an induced voltage in a tuned resonator.

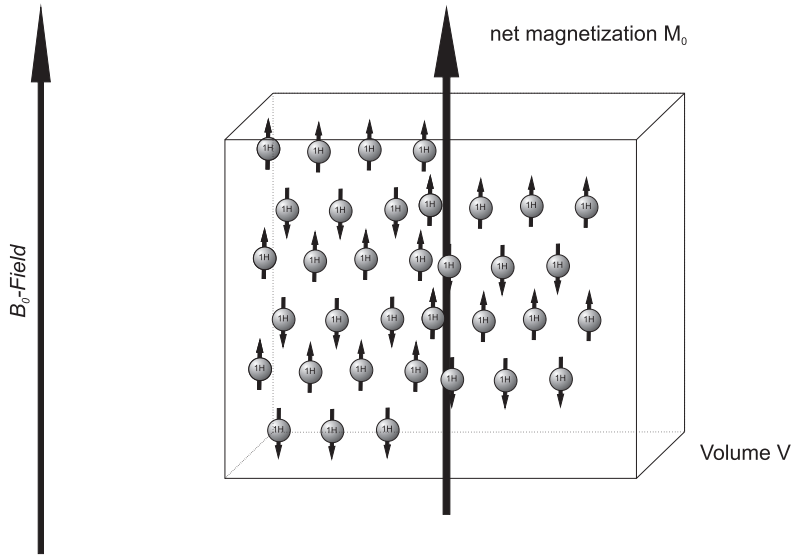

Figure 1.6: Proton spins in the presence of an outer magnetic field forming a spin system in the volume V with a net magnetization M_0.

To facilitate understanding, it is possible to change to a frame that rotates with the angular frequency ω around the z-axis of the laboratory frame. In this frame, the magnetization M is split-up into the two components M_z and M_{xy}.
If an RF field is then applied during the time t_p the magnetization is rotated by the flip angle

$$\alpha = \omega_1 t_p = \gamma B_1 t_p.$$

It is therefore possible to tilt the spin system out of equilibrium with RF power. Angles of from $0-180$ are allowed for this operation, thus allowing more or less excitation of the spin system. If the duration t_p of the RF field is chosen to rotate the magnetization in the rotating frame by 90 degrees, then this pulse is denoted as a 90 degree or $\pi/2$ pulse. Accordingly, the magnetization M is rotated by 180 degrees when the duration of the RF pulse is doubled at the same flux density B_1. This pulse, which inverts the magnetization from the positive to the negative z-direction, is called a 180 degree or π pulse.

To get spatial information, magnetic field gradients are applied in all three dimensions, see figure 1.7. Due to these gradient fields the precession frequencies of the protons can be related to points in space and the phase and frequency of the precessing magnetization can be measured by an RF resonator.

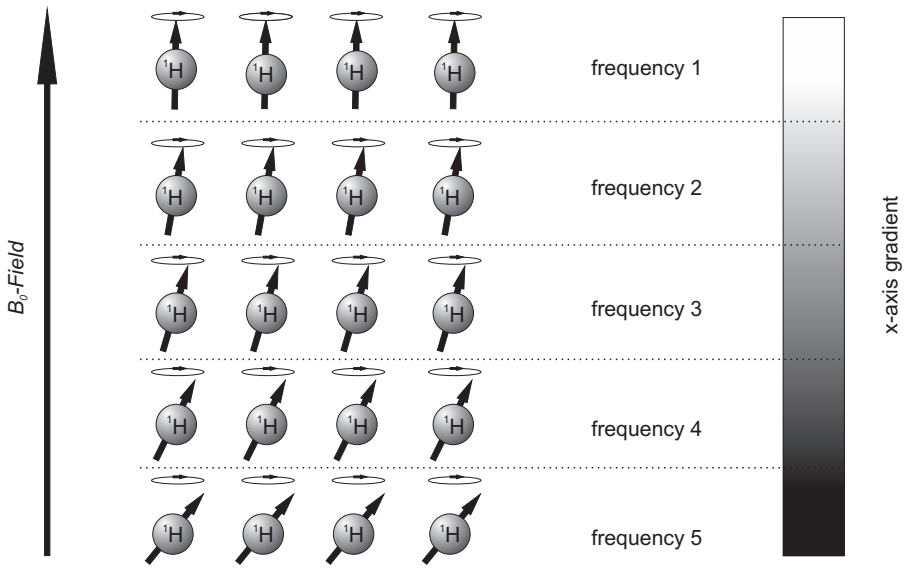

Figure 1.7: Frequency difference due to the presence of magnetic gradient field that is acting on the precessing proton spins in order to get spatial resolution. The frequency differs from slice to slice because of a slightly different B_0 value due to the gradient.

The induced signal in the resonator is then digitized and processed with an inverse two-dimensional Fourier transform to convert the signal into the spatial domain that will produce the picture.

For an in-depth introduction to magnetic resonance imaging the reader is referred to textbooks like [12].

1.4. CONVENTIONAL RF COIL DESIGN

CONVENTIONAL radio frequency (RF) coil design started in the 1950s when Gersch and Loesch [10] conducted their experiments on nuclear magnetic resonance (NMR) samples in an oscillating magnetic field. The main difference between an RF coil and an antenna is that an antenna is built to be a perfect radiator. This means that as much as possible of the amount of power applied to the antenna's terminals shall be radiated away from the antenna into free space into the far field region of the antenna. An RF coil on the other hand, tries to establish an oscillating magnetic field to excite the spin system. Here, the goal is to maximize the strength of the magnetic field in a very close vicinity to the coil that is usually within or less than a wavelength of the applied radio frequency. While on a transmit antenna, for example for a terrestrial music station in the very high frequency band (VHF), the applied oscillating current at the terminals helps to radiate the wave away by producing alternating magnetic (H) and electric (E) waves that are perpendicular to each other; on a RF coil this effect is usually unwanted. Radiated power in an MRI coil is a loss mechanism and thus decreases efficiency. The E-field is a rather annoying companion of the H-Field for the RF coil designer, as the E-field is to be blamed for dielectric interactions with human tissue that causes unwanted heating. This is why the amount of radio frequency radiation that is transmitted into the human body during an MRI exam is limited and needs to be monitored. Moreover, international guidelines exist that set-outlimits for the maximum amount of power that shall be applied to a human body. These values are usually referred to as the specific-absorption-rate (SAR).

In a simple embodiment, a radio frequency coil can be formed from a capacitor and an inductor as in figure 1.8. The capacitor stores electrical energy of an E-field, while the conductor L stores energy in the form of an H-field in its vicinity. While the mechanisms by which these devices operate are interesting, a discussion hereover is beyond the scope of this introduction – the interested reader is referred to the literature; see, for example [11] – it is further interesting to note that the storage capacity of the capacitor depends not only on its physical dimensions but also on the dielectric material used between its plates. The operating angular frequency ω of such a simple antenna (in MRI it is also referred to as a loop coil) is given by equation 1.2

$$\omega = \frac{1}{\sqrt{LC}} \tag{1.2}$$

where L is the inductance in Henry and C the capacitance in Farad. The angular

frequency ω can easily be converted into the unit for oscillations per second – Hertz – by division by 2π.

In order to use such a coil for NMR or MRI, it would have to be coupled to the transmitter and receiver by appropriate means, so that the impedance at the loop terminals would be matched to the system impedance; this is in order to allow maximum power transfer. This procedure is usually referred to as matching and can be realized either inductively or capacitively. The process of impedance matching is well described in the literature [26]. Furthermore, the angular frequency ω must be match with the resonance frequency of the NMR or MRI system ω_{system}, as given by equation 1.3

$$\omega_{system} = \gamma B_0 \tag{1.3}$$

where γ is the gyromagnetic ratio and B_0 the main magnetic field strength, for example 3.0 Tesla. Here γ is a physical constant that is dependent on the nucleus under investigation. The value for γ of the ^{1}H nuclei, for example, is 267.513×10^6 rad $s^{-1} T^{-1}$. It can thus be easily shown that the resonance frequency ω_{system} of a 3.0 Tesla MRI system must be 802.539×10^6 rad s^{-1} which equals ~128 MHz.

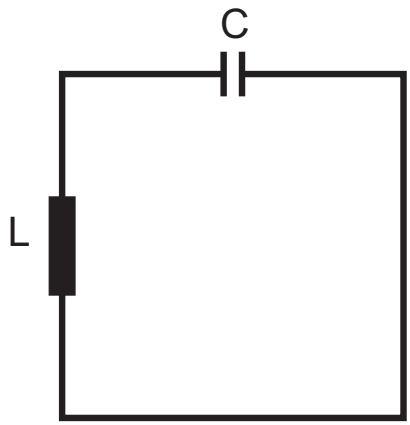

Figure 1.8: Most simple form of a radio frequency circuit (in MRI also called coil) consisting of an inductor L and a capacitor C. The capacitor C can store electric energy and the inductor L can store magnetic energy. The circuit can resonate at a resonance frequency ω that depends on the values of the inductor and capacitor.

TRANSMIT CASE

The RF-resonator, also often referred to as the coil, acts as an antenna in the near-field that converts the cable-bound electric energy to a free-air electromagnetic near-field wave. It is most desirable that all power coming from the amplifier is transferred into free space to avoid losses. Therefore, parts of the spectrometer should be connected with little to no losses. This is achieved by using 50 Ohm coaxial cables, and by adjusting the load to 50 Ohms by matching and tuning of the coil. The coil behaves then as a pure resistive load during transmission. As can be shown easily, the maximum power from a source with impedance Z_0 is transferred to a load when Z_l is the complex conjugate to the impedance of the source $Z_0 = Z_l^*$.

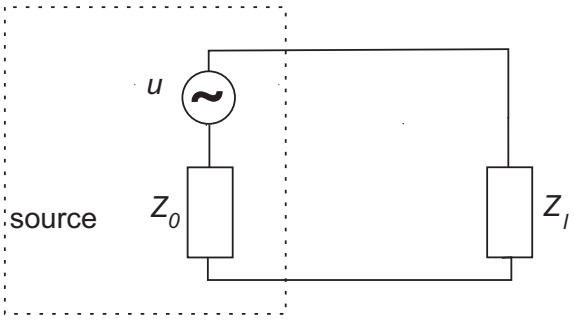

Figure 1.9: Equivalent electrical circuit of source and load in a MRI system.

It can be shown that the dissipated Power P_{loss} is

$$P_{rad} = \frac{U_0^2 Re\{Z_l\}}{|Z_0 + Z_l|^2},$$

with $U_0 = \frac{U}{\sqrt{2}}$.

It is obvious that the maximum power is transferred when the right-hand side of the equation is maximum. This is the case when

$$Re\{Z_0\} = Re\{Z_l\}$$

and

$$Im\{Z_0\} = -Im\{Z_l\}$$

The total power delivered then is

$$P = Re\{UI^*\} = \frac{U_0^2}{4Re\{Z_0\}}.$$

This also explains why all components of a RF system should have the same impedance and should be connected via lines with the same impedance. It also explains why, at best, only 50 percent of the available power can be transmitted from the source into free air.

The equations above further explains why an antenna designer must, at the same time as designing an antenna, also design a matching network if the impedance of the antenna and the line are not equal (as is usually the case). The matching network transforms the impedance and makes it possible that the source sees a perfect match on the end of the line, instead of a mismatched antenna. The same is true for the antenna; also here the matching network makes the line look like a perfect match for the antenna's own impedance. Thus, a maximum of power transfer can be achieved even though the source, line, and the antenna do not have the same impedance.

RECEIVE CASE

The receiver chain consists of an NMR-probe and a pre-amplifier: shown schematically in figure 1.10.

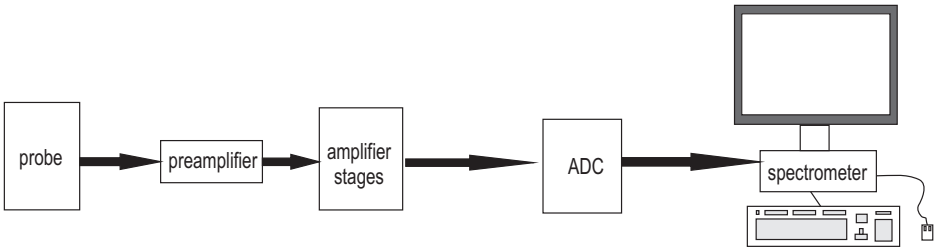

Figure 1.10: Amplifier stages. The weakly induced MRI-signal within the coil needs to be amplified to a level where digitization can take place.

Relaxation of spins in the tissue causes a current to be induced in the RF-resonator that is then amplified by the pre-amplifier. The signal is then fed through further amplification stages and after several steps of amplification, is digitized and fed into the spectroscope computer.

frequency [MHz]	free space wave length [cm]	cable velocity	fraction of wavelength λ	wavelength in cable [cm]	phase [deg]
64	469	0,666	1	313	360
			1/2	156	180
			1/4	78	90
			1/8	39	45
123	244	0,666	1	162	360
			1/2	81	180
			1/4	41	90
			1/8	20	45
298	101	0,666	1	67	360
			1/2	34	180
			1/4	17	90
			1/8	8	45

Table 1.2: Frequency, wavelength in free space and in a cable as well as the phase for frequencies relevant for magnetic resonance imaging.

1.5. IMPLICATIONS OF UHF MRI ON RF COIL DESIGN

WHILE the aforementioned considerations hinder the triumphal march of 7.0 Tesla MRI systems into clinical routine, the new ultra-high field (UHF) MRI systems ($> 7.0T$) also bring possible advantages besides their inherent high signal to noise ratio. These new high field systems run at 7.0 Tesla B_0 field strength, which gives, according to 1.3, a system B1 frequency of around 300 MHz. In this frequency regime, new solutions to RF problems become available that were not practicable at the rather low frequencies used in 1.5 and 3.0 T systems. At higher frequencies, the wavelength decreases as shown as in the table below. At shorter wavelength, micro-strip technology can be used; for example, at 300 MHz, a branch line coupler becomes a reasonable size. The 300 MHz RF devices can be shrunk even further if a substrate with a high permittivity is used. This allows for new designs and the transfer of solutions known from traditional microwave RF engineering. The origin of these advantages become clear when MRI systems of different field strengths and their associated transmit frequencies are compared. As further illustration, the wavelengths for a 1.5 Tesla (frequency 64 MHz), 3.0 Tesla (frequency 128 MHz) and a 7.0 Tesla MRI system are given in the table 1.2:

In RF circuit design, the wavelength of the system needs to be taken into consideration. Due to the large wavelength of several meters both in 1.5 and 3.0 Tesla MRI, certain elements need to be built from equivalent lumped circuit elements. For example, a 90-degree phase shift at 64 MHz would require a cable that is 78 cm long. It is not very

practical to integrate such a long cable into a circuit. Such long cables pose a threat for the patient and can cause spurious RF behaviour if not shielded properly. Thus, at 1.5 or 3.0 Tesla, when, for example, a $\lambda/4$ transmission line section is needed in a RF circuit, an equivalent lumped element circuit is used instead. This design process is schematically given in figure 1.11.

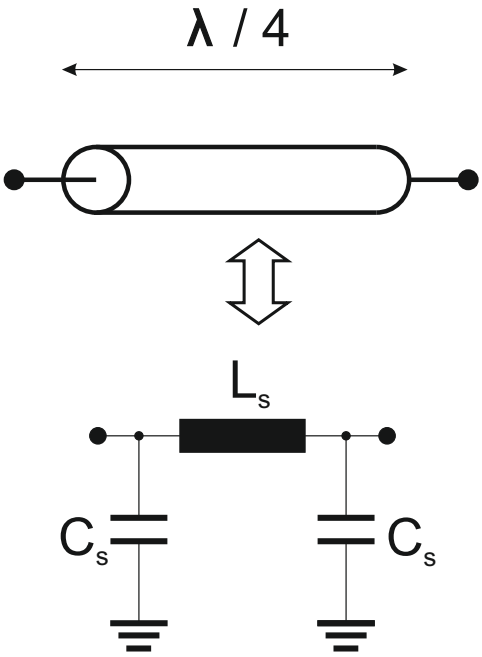

Figure 1.11: Transformation of a $\lambda/4$ transmission line into an equivalent lumped element circuit.

Designing and building such equivalent networks can be cumbersome. While in most cases there are formulas to calculate the relevant values,practical implementation is usually not straightforward (due to unavoidable random tolerances of real world elements and parasitic effects) and manual "tweaking" is often required.

At 7.0 Tesla and above, on the other hand, the working frequency becomes so high, that it is possible to use micro-strip-line technology and place the circuit parts inside the bore of the MRI. These circuits can be further reduced in size if a high permittivity carrier substrate is selected.

1.6. DIELECTRIC RESONATOR ANTENNAS

IN order to understand the concept of dielectric resonator antennas (DRAs), it is important to first know what a dielectric material is. A short answer to the question "What is a dielectric material?" would be:

"A dielectric material is an electrical insulator that can be polarized by an applied electric field."

However, a deeper understanding of the properties of matter are desirable, especially when matter is interacting with an electric field. A short introduction is thus given hereafter. For an in-depth analysis the reader is referred to classical textbooks on electrostatics such as [11, 17].

1.6.1. DIELECTRIC MATERIALS - INSULATORS AND CONDUCTORS

Matter can be subdivided into two classes: conductors and insulators (dielectrics). Conductors consist of an "unlimited" stock of charge carriers that are able to move within the conductor. For example, in metals, one or two electrons of one atom are not bound, but can move freely within the material. In dielectrics, all charge carriers are bound to atoms or molecules. They have only limited mobility in close proximity to the atom or molecule. Since those movements are very small when compared with a conductor, the effect of an external electric field on a dielectric is fundamentally different to its effect on a metal. When a metal gets exposed to an external electric field, the free charge carriers inside the metal will form a shield at the boundary of the metal that is equal in magnitude to the external applied electric field. Due to this effect, an electromagnetic wave can penetrate into a metal only for a very short distance, known as skin depth δ_s. The skin depth depends on the frequency of the incident electromagnetic wave as well as on the conductivity of the metal. We can calculate the skin depth δ_s according to [17] as

$$\delta_s = \sqrt{\frac{2}{\mu\sigma\omega}} \tag{1.4}$$

where $\omega = 2\pi f$ is the frequency in radians per second, μ the permeability in Henry per meter and σ the conductivity of the metal in Siemens per meter. The skin depth is also the reason why in MRI we can use very thin layers of copper as a coil conductor.

1.6.2. DIELECTRICS IN AN EXTERNAL ELECTRIC FIELD

When a quasi-neutral atom is moved into an electric field, it is influenced by the external field as follows: the positively charged core of the atom is displaced in the direction of the external field;the electron cloud of the atom, which is negatively charged, is displaced in the opposing direction. If the external field is strong enough, the atom can be ripped apart; a process that is called ionization. If ionization occurs, the matter becomes a conductor. If the force of the external field and the forces between the core and the electron cloud are weaker, an equilibrium is established, leading to a polarized atom having a small dipole moment p that has the same direction as the external field E. This induced dipole moment p is proportional to the external field E and can be described by

$$p = \alpha E \tag{1.5}$$

where α is a measure of how "polarizeable" an atom is. As α is about $2\pi\epsilon_0 r\text{^}3$, where r is the atom radius, we can conclude that except for the factor ϵ_0 the polarization depends on the volume of the atom.

In molecules the situation is a bit more complex as some molecules can be more or less polarized depending on the orientation of the molecule with respect to the applied external electric field. This is for example the case for carbon dioxide.

If a polar molecule such as hydrogen dioxide (water) is put into an external field, a torque is experienced by the molecule. If the molecule can rotate freely it will rotate until it is aligned with the external electric field. If the external field is removed random movement due to temperature of the material will lead to a depolarization and thus back to a net zero field. Both effects lead to polarization that can be quantified as the dipole moment per unit volume.

For many dielectric materials the amount of polarization P is proportional to the applied external electric field. It can be expressed as

$$P = \epsilon_0 \chi_e E \tag{1.6}$$

wherein χ_e is the electrical susceptibility of a dielectric and ϵ_0 is a term factored out of χ_e. It thus follows that the displacement current D in a linear media is

$$D = \epsilon_0 E + P = \epsilon_0 E + \epsilon_0 \chi_e E \tag{1.7}$$

and thus D is also proportional to E:

$$D = \epsilon E \tag{1.8}$$

with

$$\epsilon = \epsilon_0(1 + \chi_e). \tag{1.9}$$

ϵ is constant known as the dielectric constant or permittivity of a material. In vacuum the susceptibility is zero and thus the dielectric constant is ϵ_0. This is also known as the dielectric constant of a vacuum and has a value of $\epsilon_0 = 8.854 \times 10^{-12}$F/m. One can remove the factor ϵ_0 to obtain a dimensionless number:

$$\epsilon_r = 1 + \chi_e = \frac{\epsilon}{\epsilon_0} \tag{1.10}$$

this is known as the relative dielectric constant of a material.

1

1.6.3. THE LEYDEN JAR

An alternative way to describe the permittivity is to look into historic experiments. Especially the Leyden jar that was invented in the town of Leiden is very suitable for this purpose. In 1745 Pieter van Musschenbroeck [40] in Leiden and Ewald Georg von Kleist discovered independently that charges from an electrostatic generator could be gathered and stored in jar-like devices similar to the one shown in Figure 1.12.

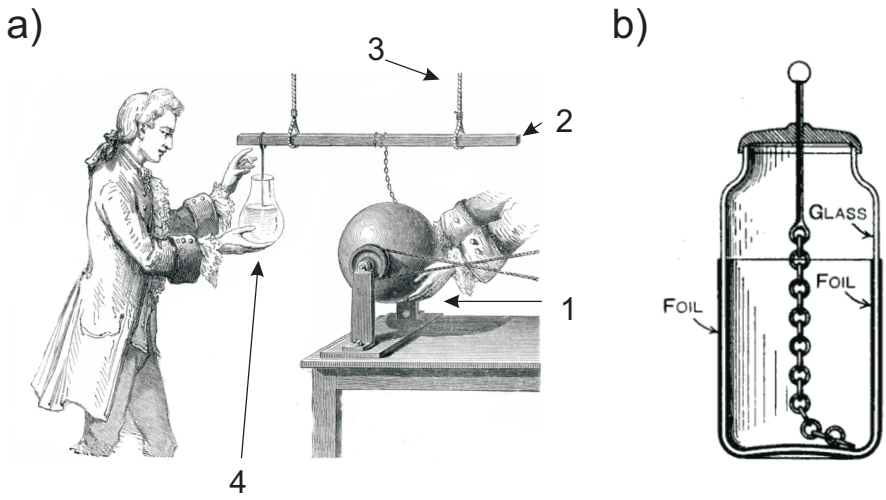

Figure 1.12: a) shows the use of a Leyden jar (4) that is used to store electrostatic energy produced by the electrostatic generator (1). Both devices are connected to each other over conductive elements like the iron bar (2) that is isolated to earth by suspension with ropes (3). b) shows a detailed view of a Leyden jar as they were commonly used until the beginning of the 20th century consisting of a jar that has a metal foil on the inside and outside. The charge is passed through a non-conductive top via a metal rod. The charge is conducted to the inner foil via the central metal chain.

For the first time in history it became possible to store electric charge and accumulate charge of a significant amount. Before the invention of this device only limited amounts of charge could be generated and stored for experiments. The Leyden jar paved the way for the experiments of Galvani, Volta, and Franklin and was widely used in the electromagnetic research community until the 20th century.

The Leyden jar acts as a basic capacitor, wherein the glass of the jar acts as a dielectric. The similarities between the Leyden jar and the parallel plate capacitor are obvious and the working principle is the same. The parallel capacitor is explained in detail in the next section.

1.6.4. THE PARALLEL PLATE CAPACITOR

The Leyden jar basically works in the same way as a parallel plate capacitor as shown in figure 1.13.

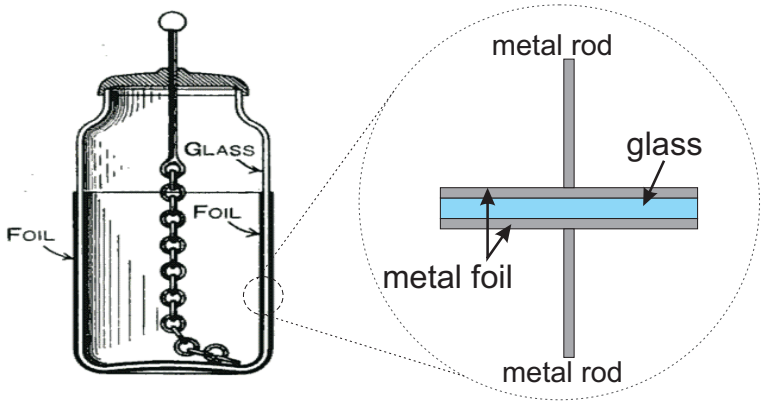

Figure 1.13: From the Leyden jar to the parallel plate capacitor. If one looks closely at a section of the Leyden jar we see a resemblance to a parallel plate capacitor: The inner and outer foil are the metal plates of the capacitor. The glass of the jar acts as a dielectric. The two metal rods are realized by the inner connector inside the jar that is conductively coupled to the charge generator. The second rod of the parallel plate capacitor is a ground connection in case of the Leyden jar usually via the experimentalist or environment.

A Leyden jar can be represented by the following model: two metallic plates with a surface area A are separated by a distance D from each other as in figure 1.14. The space in between those plates is filled with a non-conductive material such as air or vacuum. The capacitance C_0 can be determined with the equation:

$$C_0 = \frac{\epsilon_0 A}{D} \tag{1.11}$$

where ϵ_0 is the permittivity of free space, A the surface area of the plates and D the distance between the plates.

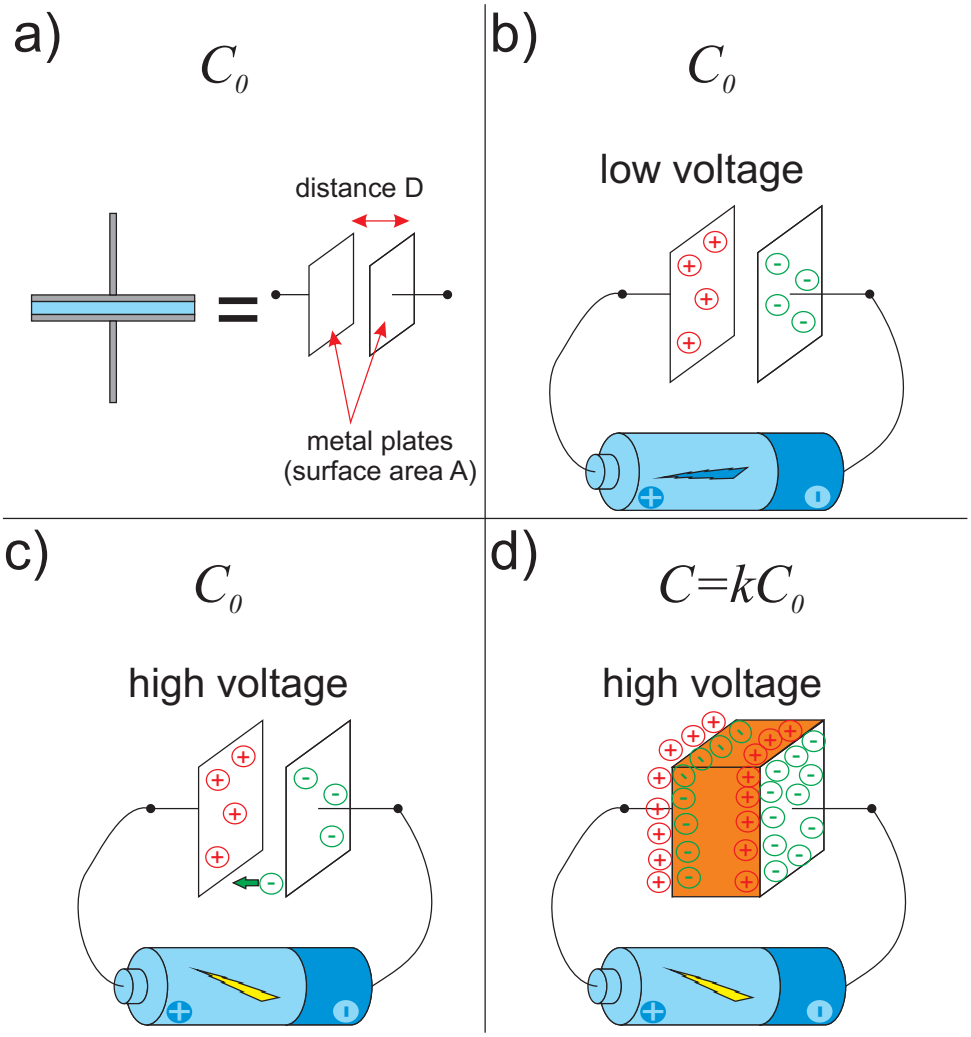

Figure 1.14: In a) we can see that the Leyden jar unit capacitor can be translated into a parallel plate capacitor with two metal plates with the surface area A that are separated by a distance D. In b) the space between the metal plates is filled by vacuum with a dielectric constant of ϵ_0 and the capacitance is C_0. When a low voltage is applied charge of opposite polarity will accumulate on the plates and create and electric field between the plates. In c) the voltage is increased to a high voltage. The high voltage allows an electron to leave its plate. If this occurs in air the air will become ionized and a spark can be observed. The capacitance is still C_0 however in the case when sparking happens the capacitor actually becomes a short and thus $C_0 = 0$ In d) the same high voltage as in c) is applied however the free space between the plates of the capacitor is now filled with a dielectric. The dielectric is polarized thus the capacitance is increased by a factor k. The new capacitance is then $C = kC_0$

If a voltage is applied to such a capacitor from a voltage source, such as a battery, the plates will become charged. One plate will become positively charged, while the other

plate accumulates the negative charges. This separation of charge causes an electric field to be generated between the plates. If the applied voltage is high enough, the air between the plates can become ionized; charge equalization via a spark can result. From a practical point of view, it is desired to prevent sparking. This is achieved by placing an insulator between the plates. The advantages are twofold: 1) the capacitor can be charged with/to a higher voltage and 2) the capacitance is now increased from C_0 to C by a factor of k e.g. more energy can be stored by the capacitor. The applied electric field leads to small displacements of atoms, ions and/or changes in orientation thereof leading to "polarization". The extent to which a material can be polarized is expressed by its permittivity or the dielectric constant. The capacitance C is then determined by:

$$C = C_0 k = \frac{k\epsilon_0 A}{D} \tag{1.12}$$

where k is a proportional factor depending on the insulating material. If we define $k\epsilon_0$ to be the permittivity of the insulator and name it ϵ we can now define the capacitance C as:

$$C = \frac{\epsilon A}{D}. \tag{1.13}$$

We have now defined the permittivity of the insulator to be ϵ, we may also equally refer to it as the dielectric constant of the insulator. It is custom to represent the dielectric constant relative to the dielectric constant of vacuum:

$$\epsilon_r = \frac{\epsilon}{\epsilon_0} \tag{1.14}$$

where ϵ_r is now the relative dielectric constant of a material, ϵ is the dielectric constant of the material and ϵ_0, the permittivity of vacuum ($\epsilon_0 = 8.854 \times 10^{-12}$F/m). It should be noted that the term dielectric constant is in fact not correct as it implies a true natural constant like Boltzmann's or Planck's constant. However, the dielectric constant is dependent on the frequency and on the temperature. It is thus preferable to use the term permittivity. While this behavior is very interesting it is of little practical importance in the frequency and temperature regimes of current human MRI. The interested reader is thus referred to textbooks on solid-state physics that cover this topic in detail such as [34] or [14].

Dielectric materials interact with electromagnetic waves. If a electromagnetic wave travelling in free space for example enters a material with a high permittivity the wave-

length decreases by a factor of $\sqrt{\epsilon_r}$. If the wave moves from one material into a second material with a different permittivity, a part of the wave will be reflected, and a part transmitted. For a more detailed description of this phenomena, see textbooks in electrical engineering or electrodynamics for example [17, 26].

Typical values of ϵ_r range from 1 to 10 for polymers, from 10 to 100 for polar solvents (with water around 80) and from 100s to thousands for inorganic compounds like perovskites. A perovskite is a material with the type of ABX_3 structure such as calcium titanate oxide [39]. One well-known perovskites is barium titanate - a dielectric ceramic. Its dielectric constant can be as high as 7000. The structure of barium titanate is given in figure 1.15.

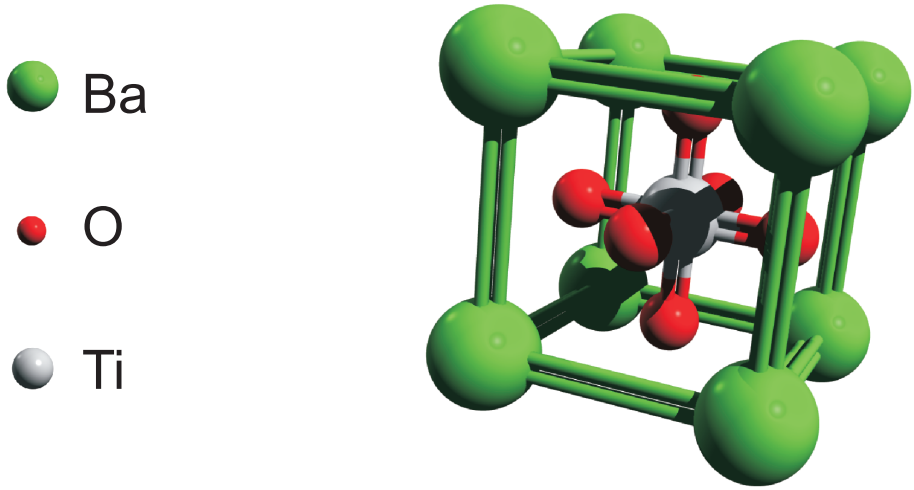

Figure 1.15: Illustration of the perovskite ABX_3 structure on the example of $BaTiO_3$.

Dielectric materials with a high permittivity, low loss and temperature stability are important for the global communications industry; they are commonly used in wireless technology for example in wireless communications base stations. For an introduction to this matter see [41]. High permittivity materials are also interesting candidates for RF coil design because they make efficient electromagnetic field storage devices and their incorporation into a conventional RF coil can significantly change the distribution of magnetic and electric fields within a sample.

1.6.5. HISTORY OF DIELECTRIC RESONATORS

DIELECTRIC resonators (DRAs) were first theorized in 1939 by Richtmyer [33]. Based on the discovery that a cylinder of dielectric material can serve as a guide for electromagnetic waves of certain frequencies he concluded that if such a cylinder would be bent and the ends joint together as in 1.16 such an object would act as an electrical resonator.

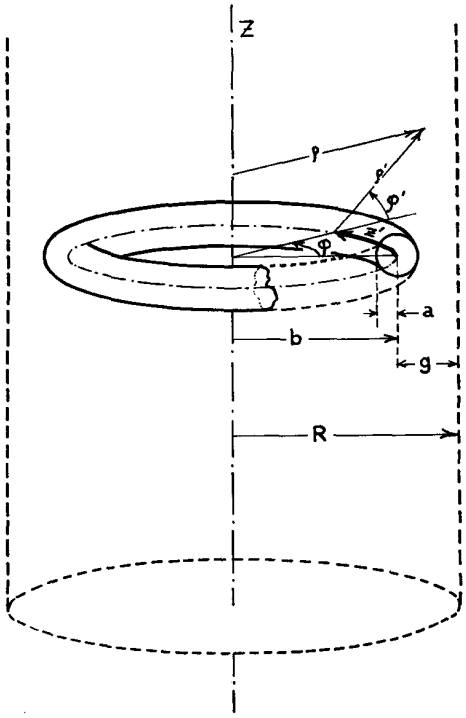

FIG. 2. Dielectric ring resonator, and various quantities used in the analysis: true cylindrical coordinates ρ, z, ϕ; pseudo-cylindrical coordinates ρ', z', ϕ'; and dimensions.

Figure 1.16: Illustration of the dielectric ring resonator suggested in the publication of Richtmyer in 1939 [33].

The description of dielectric resonator modes by Okaya and Barash [24] in the 1960s as well as the development of low loss ceramic materials in the same decade allowed for the first application as high-Q elements for circuit applications such as in filter and oscillator design. Sager and Tisi [35] were the first to mention the possibility to construct very small antennas using dielectric resonators. A more detailed overview of the development of dielectric resonators is given by Petosa in [25].

1.6.6. INTRINSIC FEATURES OF DIELECTRIC RESONATORS

Dielectric resonators offer attractive features:

- very high quality factor if used in shielded applications such as filters and oscillators with $Q_{unloaded} = \frac{1}{tan\delta}$
- effective radiators when in an unshielded environment
- dimensions in the order of $\lambda_0/\sqrt{\epsilon_r}$ where λ_0 is the free-space wavelength and ϵ_r is the dielectric constant of the resonator
- no inherent losses in conductors
- various coupling schemes exist
- various modes exist for a given geometry each with a unique internal and associated external field
- simple design formulas that can be solved using spread sheet software to design for certain dimensions or permittivity

These features make dielectric resonators an interesting candidate for MRI coil technology. DRAs are especially interesting for application at 7.0 Tesla and higher field strengths. At high field strengths, DRAs have dimensions that are more suitable compared to when applying them at lower field strengths. The effect of the B_0 field strength on the dimension of λ_0 is explained by some examples in the following table where the shortened λ_s is calculated depending on different field strength and materials:

frequency [MHz]	λ [cm]	ϵ_r	$\sqrt{\epsilon_r}$	λ_m [cm]	material
64 (1.5T)	469	80	$4\sqrt{5}$	52	water
		1000	$10\sqrt{10}$	15	perovskite
123 (3.0T)	244	80	$4\sqrt{5}$	27	water
		1000	$10\sqrt{10}$	8	perovskite
298 (7.0T)	101	80	$4\sqrt{5}$	11	water
		1000	$10\sqrt{10}$	3	perovskite

The table above shows very clearly why it is not only desirable to use materials with high permittivity for DRAs but also why it is interesting to work at a relatively high field strength.

1.6.7. MODES IN DIELECTRIC RESONATORS AND THEIR NOMENCLATURE

Dielectric resonators support stable, time-invariant electromagnetic field patterns within the resonator which are usually referred to as modes. Modes in dielectric resonators can be classified into three classes:

- Transverse electric **TE** mode
- Transverse magnetic **TM** mode
- Hybrid electromagnetic **HEM** modes

Modes are defined by the field vector that is normal to the propagation: in a TE mode resonator the electric field vector is normal to the propagation, and in a TM mode resonator the magnetic field vector is normal to the direction of propagation.

Different modes are identified by three subscripts for example a TM_{mnp} mode where m, n and p denote the number of the half-wavelength field variations in the azimuthal (ϕ), radial (ρ), and height directions, respectively. An example for the TE and TM mode is given in figure 1.17. The subscript δ is used to indicate when there is less than half-a-wavelength variation in the height direction.

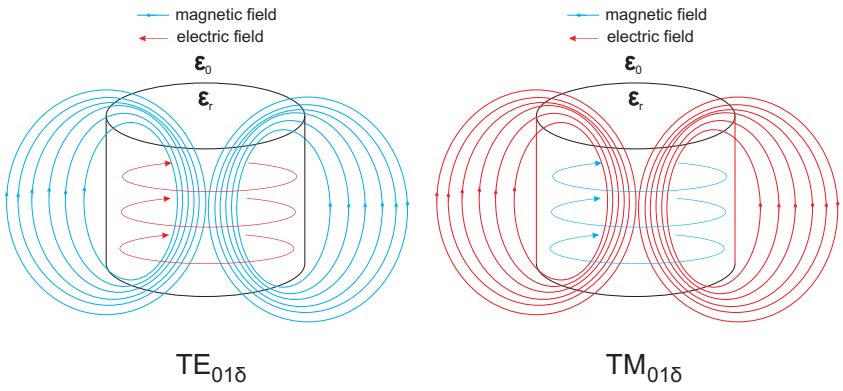

Figure 1.17: Illustration of the TE01δ and the TM01δ mode of a cylindric dielectric resonator.

1

1.6.8. DIELECTRIC RESONATOR DESIGN

Cylindrical dielectric resonators are designed by selecting their dielectric constant ϵ_r and dimension. They can take any desired shape; in practice however, rectangular or cylinder structures are usually used as the mode distributions and the resulting magnetic and electric fields are well known for these structures. These elements are usually machined into puck-like structures that can be either shielded by a metal cavity to maintain high-Q or, if the shield is removed, can become efficient antennas. Dielectric resonators are extensively used in high efficiency oscillators [18] for example. One of the obstacles in using dielectric resonators is the exact design procedure.

To estimate the correct frequency and thus mode three options are currently known:

- design based on electromagnetic simulations
- design based on empirical derived formulas
- design based on empirical experiments

Most high permittivity materials are hard and brittle. Processes for their manufacture are delicate and usually involve multiple steps. As a final step they are often sintered at high pressure and high temperature, which causes the final parts to shrink. This shrinking is not omnidirectional and thus an iterative design process might thus be needed.

A better approach, if geometrically possible, is to sinter a large block, determine the exact permittivity of the sintered block and then machine the block to dimensions that have previously been calculated. Either approach requires good knowledge of the intended final design such as the desired modal pattern, the electromagnetic field distribution for proper probe coupling, geometry and permittivity. One should decide before the design process if a fixed geometry is desired and then the permittivity is altered or vice versa. While changing the permittivity in solids is complicated, it is a rather simple exercise when using liquids as a dielectric material. Liquids can be mixed; thus the permittivity of the mixture can be adjusted. Water has a permittivity of around 80 at room temperature and, due to its natural abundance, is an interesting and inexpensive material for preliminary experiments. In order to change its permittivity, it can be mixed with alcohols for example. Unfortunately, the permittivity is very often too low for design purposes. In our laboratory an interesting alternative to solids was established involving using powdery high permittivity materials that are mixed with water to obtain thick, high permittivity slurries. These slurries can then be filled either into containers with the desired shape or even into bags

that allow conformal placement of high permittivity materials to the human body. These materials have proven very valuable for high field magnetic resonance imaging as they allow the creation of secondary B_1 fields in areas that otherwise suffer low signal intensity [36].

DESIGN BASED ON ELECTROMAGNETIC SIMULATIONS

Nowadays, electromagnetic simulation is widely available. Commercial packages exist that allow fast convergence and simple computation of resonant structures. Especially when simulating highly resonant structures, eigenmode analysis becomes a valuable tool. Electromagnetic simulation software permits modal distribution calculation over a specified bandwidth and the visualization of magnetic and electric field distribution for each of the calculated modes.

In general, two major types of three dimensional electromagnetic analysis for non-radiating structures exist:

1. driven modal analysis
2. eigenmode analysis

While the driven modal analysis uses an external excitation source via wave-ports, eigenmode analysis does not need excitation ports, as stored energy within the structure exists. The driven modal analysis yields s-parameters and the internal fields while the eigenmode analysis gives, additionally to the fields of each mode, also the natural modes and resonances. However, the eigenmode analysis does not provide s-parameters. Driven modal analysis is more often used as the computed s-parameters can be compared with those that have been obtained from a prototype of the resonator.

A characteristic of electromagnetic simulation is that it needs the geometry that the dielectric is to take as an input parameter. For a simple cylinder it is enough to specify the radius and height as well as the material properties. The boundary conditions and background material need to be set and then the simulation can be started. As there are numerous modes possible, one must specify for the simulator how many modes it shall compute. If set up correctly, one of the first modes found by the software should be the TE01δ mode. The calculation time for the first five modes of a model with about 20.000 tetrahedrons is about 20 seconds on a workstation with a single six core Intel Xeon e-1650v3 CPU equipped with 32 gigabytes of random access memory. An increased number of tetrahedrons will give a bit improved accuracy but also will make the computation

effort significantly larger. As an example, for a cylinder with radius 43 millimeters and a height of 39 millimeters filled with distilled water as a dielectric, the first five modes were calculated. The result is shown in figure 1.18.

Solver order: 2nd (constant)
Curved elements: up to order 3 (automatic)

Estimation frequency: 50 MHz

Adaptive Computation

Pass 1:

Eigenmode solver results:

Mode	Frequency	Accuracy
1	418.3124 MHz	1.252e-007
2	538.4263 MHz	1.203e-007
3	538.4678 MHz	1.312e-007
4	569.5293 MHz	2.099e-007
5	569.5693 MHz	1.748e-007

Marked 1570 of 5827 for refinement.

Pass 2:

Eigenmode solver results:

Mode	Frequency	Accuracy
1	417.6731 MHz	9.148e-008
2	538.1474 MHz	3.598e-007
3	538.1558 MHz	1.931e-007
4	569.0552 MHz	1.848e-007
5	569.061 MHz	2.127e-007

Desired accuracy limit reached, mesh adaptation stopped.

Figure 1.18: Simulation results for dielectric resonator. The first five modes have been calculated. The modes two and three as well as four and five are orthogonal modes: the have the same modal pattern but are orthogonal to each other. These modes can be fed in quadrature like the HEM11δ mode.

The software then allows also for a visualization of the single modes: both the electric field and the magnetic field can be visualized. The electric field for the first mode found from figure 1.18 is given in figure 1.19.

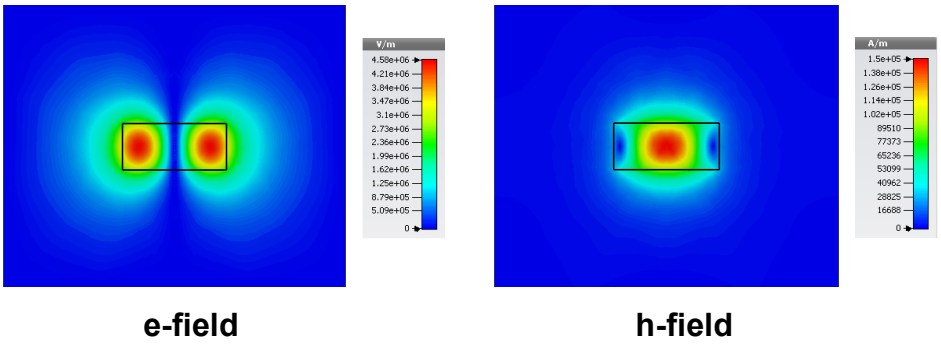

Figure 1.19: Visualization of the electric and magnetic field of the first mode of a cylindric dielectric resonator. The view shows the amplitude of the electric field (left) and the magnetic field (right) in a transversal cut plane through the cylinder.

In our laboratory we used eigenmode analysis due to its fast convergence and thus

reduced computing time. In order to verify the frequencies of the modes we measured the S11-parameter (reflection response) with a simple pickup loop attached to a network analyzer like in figure 1.20.

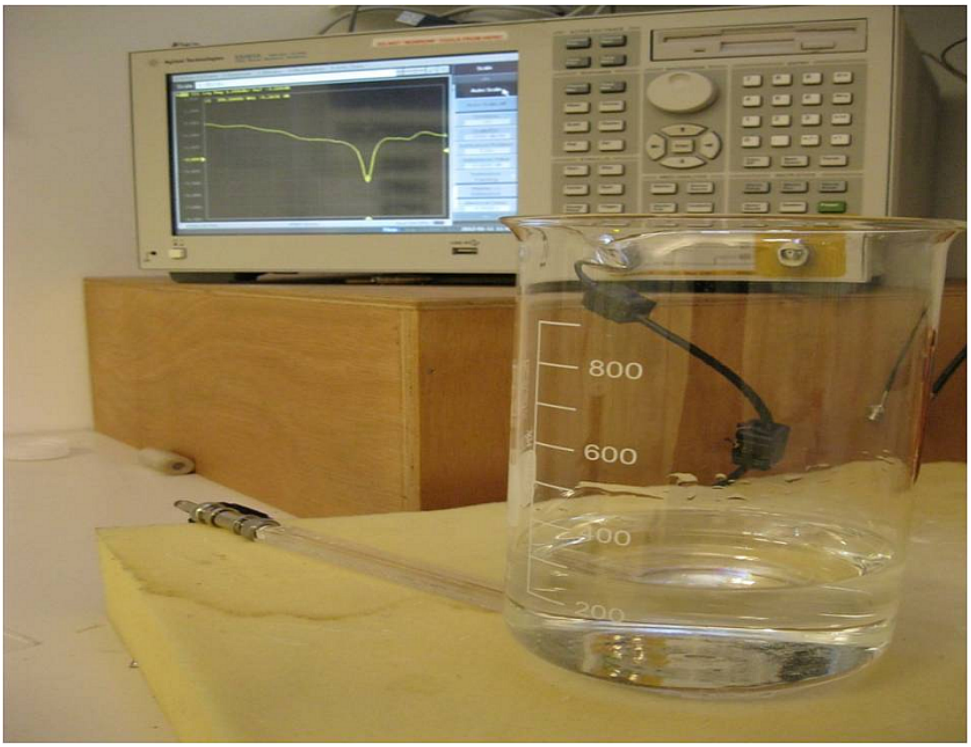

Figure 1.20: Verification of the simulation: a simple loop probe is used to couple into the dielectric resonator (in this case a beaker filled with distilled water). The S11-parameter is measured and the frequency response of the mode can be seen on the network analyser.

Eigenmode analysis is a valuable tool for the design of DRAs, but it has its limitations: due to the nature of eigenmode analysis it is for example not possible to examine a coaxial cylinder with two different permittivities. One would get only the modes for each cylinder not for the superposition e.g. the whole device. However, the coaxial case is quite interesting for magnetic resonance imaging as it represents the case when a dielectric cylinder is loaded with a human body. In those cases, one has to go back to finite difference time domain methods in order to solve the Maxwell equations to get the field distributions for such a device in the loaded case. In those simulations also, excitation ports need to be defined. So far we have implemented this via loops that couple inductively into the DRA.

DESIGN BASED ON EMPIRICAL DERIVED FORMULAS

While closed formulas for an isolated, e.g. surrounded by a conducting wall, DRA exist, those analytical solutions are of very limited help when determing the resonant frequency of a real-world DRA [25]. However, a number of empirical derived expressions exist in the literature [19] that allow the calculation of the lowest resonant frequencies of the TE01δ, HEM11, and TM01 modes for cylindrical DRAs:

$$f_{TE_{01\delta}} = 2.961 \frac{c\epsilon_r^{-0.465}}{2\pi a}\left[0.691 + 0.319\frac{a}{h} - 0.035\left(\frac{a}{h}\right)^2\right] \tag{1.15}$$

$$f_{HEM_{11\delta}} = 2.735 \frac{c\epsilon_r^{-0.436}}{2\pi a}\left[0.543 + 0.589\frac{a}{h} - 0.05\left(\frac{a}{h}\right)^2\right] \tag{1.16}$$

$$f_{TM_{01}} = 2.933 \frac{c\epsilon_r^{-0.468}}{2\pi a}\left[1 - \left(0.075 - 0.05\frac{a}{h}\right)\left(\frac{\epsilon_r - 10}{28}\right)\right]\left[1.048 + 0.377\frac{a}{h} - 0.071\left(\frac{a}{h}\right)^2\right] \tag{1.17}$$

where ϵ_r is the permittivity of the resonator, a the radius and h the height in meters.

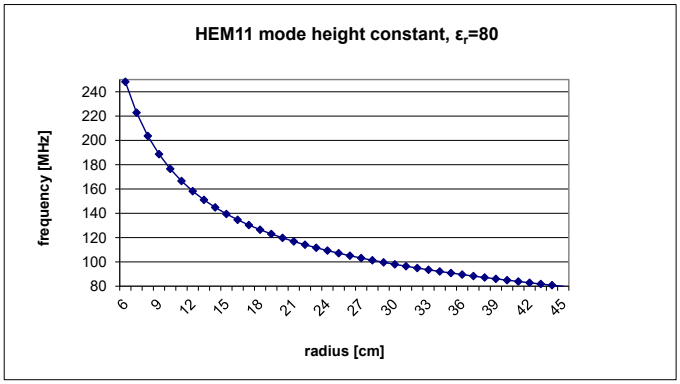

Figure 1.21: An example for a HEM_{11} mode design based on empirical derived formulas. By inserting equation 1.16 into a spread sheet simple design calculations can be made. In this example the height of the cylinder and permittivity were fixed. Now one can choose conveniently the right radius for the required frequency. This example also shows that a water based dielectric resonator would become quite large with a radius of about 20 cm.

1.7. PLASMA ANTENNAS

1.7.1. INTRODUCTION TO PLASMA

CHAPTER five of this thesis introduces a new type of magnetic resonance imaging coil that is based on plasma. As this is a new concept to the world of magnetic resonance imaging a brief introduction into plasma is given here.

The English physicist Sir William Crookes suggested in 1879 [8], while considering the properties of matter in electrical discharges, that these gases are the fourth state of matter. The terminology follows the idea that changes in the state of matter can be achieved by adding energy, for example in the form of heat as shown as in figure 1.22. The term plasma was first introduced by Tonks and Langmuir [38] in the 1920s.

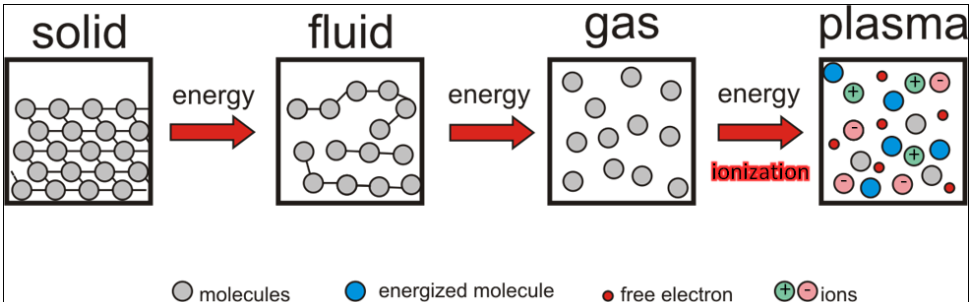

Figure 1.22: Plasma as the fourth state of matter: by adding energy to a solid first a liquid state is created which goes into a gas state if further energy is added. If even more energy is added the molecules in the gas start to ionize thus the gas becomes a plasma. While in the first three phases molecules and atoms move as one unit in the plasma phase ions and electron move separately. Instead of energy or heat one can also define the state of matter by the average kinetic energy per particle.

A gas which is normally an electric insulator becomes a good electrical conductor when it is turned into a plasma. This is because in a plasma a large number of free electrons and positive ions exist alongside neutral atoms and molecules. These electric charges can move freely and are responsible for the electric conductance of the plasma and the quasi-neutrality of plasma. The amount of ionization of a plasma can be described by the ratio of $n_e/(n_e+n_n)$ where n_e is the number of electrons and n_n the density of neutral atoms. The amount of ionization in a fluorescent tube for example is of the order of $\sim 10^{-5}$. A plasma is considered weakly ionized if the degree of ionization is less than 10^{-4}.

The plasma inside a confinement chamber is quasi-neutral because where the plasma

faces a boundary a sheath is formed as shown as in figure 1.23. The effect is similar to metals, that are inside potential free when exposed to an external electric field after a certain distance (also known as the skin depth effect). The sheath shields the inner plasma from the electric field as charge is allowed to concentrate in close proximity to the boundary.

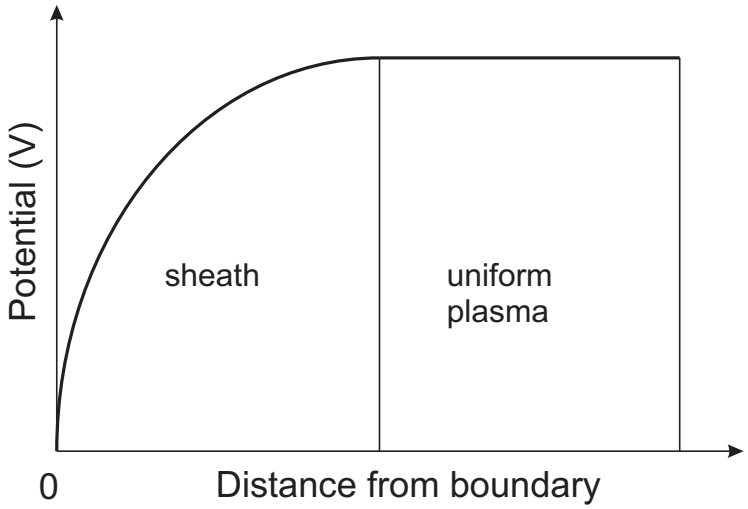

Figure 1.23: A plasma forms a sheath at its borders. While inside the plasma quasi-neutrality is given there is a difference in potential at the border of the plasma. In the sheath region electrons form a shield against the boundary. This means that positive ions will not reach the plasma wall and can thus not leave the plasma. The sheath is a conducting outer layer that is capable of guiding surface waves.

Usually a plasma is described in terms of pressure, density and temperature using statistical mechanics. It is common to classify plasmas according to their density and temperature. The pressure in a plasma is usually calculated by

$$P = \rho T \tag{1.18}$$

where P is the pressure, ρ is the density and T is the temperature.

In general, the forces between the charges inside a plasma can be described using Coulombs law. In a plasma, a positive ion will be surrounded (shielded) by an electron cloud. Coulomb's law does not take shielding of charged particles into account as the several shielding layers restrict the force of attraction of the ion to a finite distance and

not infinity. The shielding of a single charged particle that is taking place in plasmas is the same as in liquids containing ions as has been described by the Dutch physicist Peter Debye. As the shielding of one positive ion is omnidirectional in space, it describes a sphere around the ion, this effect is known as Debye shielding. The aforementioned statements are true for weakly ionized plasma. In a fully ionized plasma the particles are subject only to Coulomb collisions. It is possible, according to [15] to calculate the Debye length λ_d for cases where the ions mobility is negligible as

$$\lambda_d = \sqrt{\frac{\epsilon_0 k_b T_e}{n_e q_e^2}} \tag{1.19}$$

with ϵ_0 being the permittivity of free space, k_b is Boltzmann's constant, T_e the electron temperature, n_e the electron density and q_e is the electron charge.

It is furthermore known that the electrons in a plasma are collectively oscillating, a motion that can be described using wave equations. The ions in the plasma are also moving collectively in a wave form, however at a lower frequency. The collision frequency depends on the 'mean free path' which is defined as the average distance a particles travels between collisions within its medium. The collision frequency is inversely proportional to the density of the medium. The mean free path in solids is usually smaller than in a liquid and much smaller in a gas. As in a plasma mean free paths can be similar to all those three states of matter, also the cross section is invoked to describe the probability of collision. As charged particles are investigated, the cross section is not based on geometry but rather by using the effective area of the electric forces, as this also takes relative speed of the particles into account. The oscillations that arise from disturbances from equilibrium can be described as an angular frequency ω_p (also known as plasma frequency) with

$$\omega_p = \sqrt{\frac{n_e q_e^2}{\epsilon_0 m_e}} \tag{1.20}$$

where n_e is the electron number density (measured in m^{-3}), m_e the electron mass, ϵ_0 the permittivity of free space, and q_e the electron charge. The plasma frequency determines the behaviour of the plasma with respect to electromagnetic waves.

The field of plasma physics is a complex field and the reader can find more information in [1, 13] and [15].

The idea of using plasma as antennas is not entirely new and has been tried in the

fields of communication and radar before [3, 4]. The main reason to use plasma in such fields are the unique properties that plasma antennas offer:

- small radar cross-section when the plasma antenna is not energized
- reconfiguration of the transmit and receive bandwidth by reconfiguring the plasma
- lower noise levels than metal antennas if needed
- plasma can be switched off and on as needed

The plasma can be formed by two electrodes like in AC-mains lighting. However multiple other means of plasma excitation exist such as:

- laser beam
- electric fields
- microwave and RF energy
- chemical process
- contact ionisation
- adiabatic compression
- electron beam
- beam of particles

A well written overview of possible excitation technologies can be found in the publication from Conrads [7].

Yet another interesting means of excitation was suggested by Moisan [22] and Burykin [5]. A plasma column can be excited by a surface wave that is driven from one end of a column. This surface wave can travel along the plasma column for frequencies lower than the plasma frequency. According to Borg [4], the current induced by the surface wave along the column can, under the right circumstances, be very similar to that of a wave propagating on a metallic dipole antenna. This makes plasma columns (that can be used as a mono- or dipole) an interesting candidate for use in high field MRI where several new coil designs using dipoles have been shown to be very promising [16, 28–30, 42].

REFERENCES

[1] P. Bellan. *Fundamentals of plasma physics*. Cambridge University Press, 2006.

[2] F. Bloch. Nuclear induction. *Physical review*, 70(7-8):460, 1946.

[3] G. Borg, J. Harris, N. Martin, D. Thorncraft, R. Milliken, D. Miljak, B. Kwan, T. Ng, and J. Kircher. Plasmas as antennas: Theory, experiment and applications. *Physics of Plasmas (1994-present)*, 7(5):2198–2202, 2000.

[4] G. Borg, J. Harris, D. Miljak, and N. Martin. Application of plasma columns to radiofrequency antennas. *Applied physics letters*, 74(22):3272–3274, 1999.

[5] I. I. Burykin, S. Levitskii, and V. Martynenko. The radiation of electromagnetic waves by a variable cross section cylindrical plasma waveguide. *Radio Engineering and Electronic Physics*, 20:86–91, 1975.

[6] C. M. Collins, W. Liu, W. Schreiber, Q. X. Yang, and M. B. Smith. Central brightening due to constructive interference with, without, and despite dielectric resonance. *Journal of Magnetic Resonance Imaging*, 21(2):192–196, 2005.

[7] H. Conrads and M. Schmidt. Plasma generation and plasma sources. *Plasma Sources Science and Technology*, 9(4):441, 2000.

[8] W. Crookes. On a fourth state of matter. *Proceedings of the Royal Society of London*, 30(200-205):469–472, 1879.

[9] O. Dietrich, M. F. Reiser, and S. O. Schoenberg. Artifacts in 3-t mri: physical background and reduction strategies. *European journal of radiology*, 65(1):29–35, 2008.

[10] U. Gersch and A. Loesche. Untersuchungen der paramagnetischen kernresonanzabsorption im kondensatorfeld. *Annals of Physics*, 455(1-6):167–172, 1957.

[11] J. Griffiths. *Introduction to Electrodynamics*. Prentice Hall, 1999.

[12] E. Haacke, R. Brown, M. Thompson, and R. Venkatesan. *Magnetic Resonance Imaging: Physical Principles and Sequence Design*. John Wiley & Sons, 1999.

[13] J. Harry. *Introduction to Plasma Technology*. Wiley-VCH, 2010.

[14] P. Hofmann. *Solid State Physics: An Introduction*. Wiley-VCH, 2008.

[15] U. Inan and A. Golkowski. *Principles of Plasma Physics for Engineers and Scientists*. Cambridge University Press, 2011.

[16] O. Ipek, A. Raaijmakers, J. Lagendijk, P. Luijten, and C. van den Berg. Optimization of the radiative antenna for 7-t magnetic resonance body imaging. *Concepts in Magnetic Resonance Part B: Magnetic Resonance Engineering*, 43(1):1–10, 2013.

[17] J. Jackson. *Classical Electrodynamics*. Wiley, 1962.

[18] A. Khanna. Review of dielectric resonator oscillator technology. In *1987 IEEE International Frequency Control Symposium Proceedings*, pages 478–486, 1987.

[19] A. Kishk, A. Glisson, and G. Junker. Bandwidth enhancement for split cylindrical dielectric resonator antennas. *Progress In Electromagnetics Research*, 33:97–118, 2001.

[20] P. C. Lauterbur. Image formation by induced local interactions: examples employing nuclear magnetic resonance. *Nature*, 1973.

[21] P. Mansfield. Multi-planar image formation using nmr spin echoes. *Journal of Physics C: Solid State Physics*, 10(3):L55, 1977.

[22] M. Moisan, A. Shivarova, and A. Trivelpiece. Experimental investigations of the propagation of surface waves along a plasma column. *Plasma physics*, 24(11):1331, 1982.

[23] OECD. *Health at a glance 2015: OECD Indicators*. OECD Publishing, 2015.

[24] A. Okaya and L. Barash. The dielectric microwave resonator. *Proceedings of the IRE*, 50(10):2081–2092, 1962.

[25] A. Petosa. *Dielectric Resonator Antenna Handbook*. Artech House Publishers, 2007.

[26] D. Pozar. *Microwave Engineering*. Wiley, 2011.

[27] E. M. Purcell, H. Torrey, and R. V. Pound. Resonance absorption by nuclear magnetic moments in a solid. *Physical review*, 69(1-2):37, 1946.

[28] A. Raaijmakers and C. Berg. Antennas as surface array elements for body imaging at ultrahigh field strengths. *eMagRes*, 2012.

[29] A. Raaijmakers, O. Ipek, D. Klomp, C. Possanzini, P. Harvey, J. Lagendijk, and C. Van den Berg. Design of a radiative surface coil array element at 7 t: The single-side adapted dipole antenna. *Magnetic Resonance in Medicine*, 66(5):1488–1497, 2011.

[30] A. Raaijmakers, P. Luijten, and C. Berg. Dipole antennas for ultrahigh-field body imaging: a comparison with loop coils. *NMR in Biomedicine*, 2015.

[31] H. Rahbar, S. C. Partridge, W. B. DeMartini, B. Thursten, and C. D. Lehman. Clinical and technical considerations for high quality breast mri at 3 tesla. *Journal of Magnetic Resonance Imaging*, 37(4):778–790, 2013.

[32] T. Redpath. Signal-to-noise ratio in mri. *The British Journal of Radiology*, 71(847):704–707, 1998.

[33] R. Richtmyer. Dielectric resonators. *Journal of Applied Physics*, 10(6):391–398, 1939.

[34] M. Rogalski and S. Palmer. *Solid State Physics*. Gordon and Breach Science Publishers, 2000.

[35] O. Sager and F. Tisi. On eigenmodes and forced resonance-modes of dielectric spheres. *Proceedings of the IEEE*, 56(9):1593–1594, 1968.

[36] J. E. M. Snaar, W. M. Teeuwisse, M. J. Versluis, M. A. van Buchem, H. E. Kan, N. B. Smith, and A. G. Webb. Improvements in high-field localized mrs of the medial temporal lobe in humans using new deformable high-dielectric materials. *NMR in biomedicine*, 24(7):873–9, aug 2011.

[37] B. J. Soher, B. M. Dale, and E. M. Merkle. A review of mr physics: 3t versus 1.5 t. *Magnetic resonance imaging clinics of North America*, 15(3):277–290, 2007.

[38] L. Tonks and I. Langmuir. Oscillations in ionized gases. *Physical Review*, 33(2):195, 1929.

[39] K. Uchino. Glory of piezoelectric perovskites. *Science and Technology of Advanced Materials*, 2016.

[40] P. Van Musschenbroek. *Essai de physique*, volume 2. Chez Samuel Luchtmans, Imprimeur de l'Université, 1751.

[41] T. Vanderah. Talking Ceramics. *Science*, 298(5596):1182–1184, 2002.

[42] L. Winter, C. Özerdem, W. Hoffmann, D. Santoro, A. Müller, H. Waiczies, R. Seemann, A. Graessl, P. Wust, and T. Niendorf. Design and evaluation of a hybrid radiofrequency applicator for magnetic resonance imaging and rf induced hyperthermia: electromagnetic field simulations up to 14.0 tesla and proof-of-concept at 7.0 tesla. *PloS one*, 8(4):e61661, 2013.

[43] Q. Yang, J. Wang, and X. Zhang. Analysis of wave behavior in lossy dielectric samples at high field. *Magnetic Resonance in Medicine*, 47(5):982–989, 2002.